Underwater Target Classification Using Canonical Correlations

Ali Pezeshki, Mahmood R. Azimi-Sadjadi, Louis L. Scharf, and Marc Robinson
Department of Electrical and Computer Engineering
Colorado State University, Fort Collins, Colorado 80523–1373
Email: azimi@engr.colostate.edu

***Abstract*— A feature extraction method for underwater target classification is developed that exploits the linear dependence (coherence) between two sonar returns. A canonical coordinate decomposition is applied to resolve two consecutive acoustic backscattered signals into their dominant canonical coordinates. The corresponding canonical correlations are selected as features for classifying mine-like from non-mine-like objects. Test results are based on a subset of a wideband data set that has been collected at the Applied Research Lab (ARL), University of Texas (UT)-Austin. This subset includes returns from different mine-like and non-mine-like objects at several aspect angles in two different bottom conditions. The test results demonstrate the potential of the canonical correlation-based feature extraction for underwater target classification in difficult bottom conditions.**

I. Introduction

Detection and classification of underwater targets from sonar signals [1]-[6] involves discrimination between targets and non-targets, as well as the characterization of background clutter. The decision about the presence and type of an object is usually made based on the observation of the properties of the sonar returns at several aspect angles [5]-[7]. However, variations in the signatures of the objects and environmental conditions, the presence of heavy clutter, and several other factors complicate this process. Therefore, extracting features that are representative of spatial and temporal properties of an object at multiple aspect angles can play a crucial role in the success of the detection/classfication scheme.

In this paper a new feature extraction method for underwater target detection and classification is developed. This method exploits the linear dependence (coherence) between two consecutive sonar returns to determine whether common signatures associated with targets or non-targets are present in the corresponding returns. The idea in this approach is that the presence of a common object in two sonar returns causes linear dependence or coherence between the returns. On the other hand, in the absence of a common object, the returns from the ocean bottom are linearly independent or incoherent, provided that the aspect separation between the sonar returns is adequately large.

Canonical coordinate decompositions [8]-[10] provide an elegant framework for analyzing linear dependence between two data channels. They decompose the linear dependence between the original channels into the linear dependence between the canonical coordinates of the channels, where this linear dependence is easily determined by the corresponding canonical correlations [8],[9]. For the analysis of linear dependence between sonar returns, using a canonical coordinate decomposition, the channels may be chosen as the vectors of the time series associated with overlapping or non-overlapping blocks of range cells in two consecutive sonar returns. The canonical correlations obtained from this decomposition measure the linear dependence between the returns.

We hypothesize that the presence of mine-like-objects yields similar coherence level between sonar returns and this level is different from that caused by the presence of non-mine-like objects. The coherence level is mainly measured by the large canonical correlations of the corresponding returns. Thus, the dominant canonical correlations extracted from two consecutive sonar returns from an object may be used to classify the object at the corresponding aspect angles. We test our hypothesis on a subset of the wideband data set that has been collected at the Applied Research Lab (ARL), University of Texas (UT)-Austin. This subset contains wideband (85 kHz) sonar returns from three mine-like and three non-mine-like objects for several aspect angles in two different environmental conditions, namely, smooth bottom and rough bottom.

II. A Review on Canonical Coordinate Decomposition

Let us consider the two-channel data, $\mathbf{x} \in R^{m\times 1}$ and $\mathbf{y} \in R^{n\times 1}$ with m being the smaller dimension ($m \leq n$). It is assumed that $\mathbf{x}$ and $\mathbf{y}$ have zero means and share the composite covariance matrix

$$\begin{bmatrix} \mathbf{R}_{xx} & \mathbf{R}_{xy} \\ \mathbf{R}_{yx} & \mathbf{R}_{yy} \end{bmatrix} = E\left[\begin{pmatrix} \mathbf{x} \\ \mathbf{y} \end{pmatrix} \begin{pmatrix} \mathbf{x}^T & \mathbf{y}^T \end{pmatrix} \right] \quad (1)$$

We may write the singular value decomposition (SVD) of the coherence matrix [8], $\mathbf{C}$, as [8]

$$\begin{gathered} \mathbf{C} = \mathbf{R}_{xx}^{-1/2}\mathbf{R}_{xy}\mathbf{R}_{yy}^{-T/2} = \mathbf{FKG}^T \quad \text{and} \quad \mathbf{F}^T\mathbf{CG} = \mathbf{K}, \\ \mathbf{F}^T\mathbf{F} = \mathbf{I}, \ \ \mathbf{G}^T\mathbf{G} = \mathbf{I}, \quad \mathbf{K} = \text{diag}[k_1, k_2, \ldots, k_m]; \end{gathered} \quad (2)$$

where $\mathbf{R}_{xx}^{-1/2}\mathbf{R}_{xx}\mathbf{R}_{xx}^{-T/2} = \mathbf{I}$, and $\mathbf{R}_{xx}^{1/2}\mathbf{R}_{xx}^{T/2} = \mathbf{R}_{xx}$. We note that only nonzero singular values of $\mathbf{C}$ and their corresponding singular vectors are considered in this SVD.

The canonical coordinates of $\mathbf{x}$ and $\mathbf{y}$ are then defined as [8],[9]

$$\begin{bmatrix} \mathbf{u} \\ \mathbf{v} \end{bmatrix} = \begin{bmatrix} \mathbf{F}^T & \mathbf{0} \\ \mathbf{0} & \mathbf{G}^T \end{bmatrix} \begin{bmatrix} \mathbf{R}_{xx}^{-1/2} & \mathbf{0} \\ \mathbf{0} & \mathbf{R}_{yy}^{-1/2} \end{bmatrix} \begin{bmatrix} \mathbf{x} \\ \mathbf{y} \end{bmatrix} \quad (3)$$

This work is supported by the Office of Naval Research under contract N00014-02-1-0006.

Consequently, $\mathbf{W}^T = \mathbf{F}^T\mathbf{R}_{xx}^{-1/2}$ and $\mathbf{D}^T = \mathbf{G}^T\mathbf{R}_{yy}^{-1/2}$ are the matrices that map $\mathbf{x}$ and $\mathbf{y}$ to their corresponding canonical coordinates

$$\mathbf{u} = \mathbf{W}^T\mathbf{x} \quad \text{and} \quad \mathbf{v} = \mathbf{D}^T\mathbf{y} \tag{4}$$

The canonical coordinate vectors $\mathbf{u}$ and $\mathbf{v}$ share the composite covariance matrix

$$\begin{aligned}\begin{bmatrix} \mathbf{R}_{uu} & \mathbf{R}_{uv} \\ \mathbf{R}_{vu} & \mathbf{R}_{vv} \end{bmatrix} &= E\left[\begin{pmatrix} \mathbf{u} \\ \mathbf{v} \end{pmatrix} \begin{pmatrix} \mathbf{u}^T & \mathbf{v}^T \end{pmatrix} \right] \\ &= \begin{bmatrix} \mathbf{W}^T\mathbf{R}_{xx}\mathbf{W} & \mathbf{W}^T\mathbf{R}_{xy}\mathbf{D} \\ \mathbf{D}^T\mathbf{R}_{yx}\mathbf{W} & \mathbf{D}^T\mathbf{R}_{yy}\mathbf{D} \end{bmatrix} = \begin{bmatrix} \mathbf{I} & \mathbf{K} \\ \mathbf{K} & \mathbf{I} \end{bmatrix}\end{aligned} \tag{5}$$

The diagonal cross-covariance matrix

$$\mathbf{K} = \mathbf{F}^T\mathbf{C}\mathbf{G} = \mathbf{R}_{uv} = \mathbf{W}^T\mathbf{R}_{xy}\mathbf{D} \tag{6}$$

is the canonical correlation matrix of canonical correlations k_i; $i = 1, 2, \ldots, m$, with $1 \geq k_1 \geq k_2 \geq \cdots \geq k_m > 0$ [8],[9].

The important property of canonical correlations is that they are invariant under uncoupled nonsingular transformations of $\mathbf{x}$ and $\mathbf{y}$ [8],[10]. Moreover, some useful characteristics of $\mathbf{x}$ and $\mathbf{y}$ such as linear dependence (coherence) and mutual information are determined by their canonical correlations. Using the Hadamard ratio, the linear dependence L between $\mathbf{x}$ and $\mathbf{y}$ may be written as [8]

$$L = \det\{\mathbf{I} - \mathbf{K}\mathbf{K}^T\} = \prod_{i=1}^{m}(1 - k_i^2) \tag{7}$$

In the case where $\mathbf{x}$ and $\mathbf{y}$ are marginally Gaussian, the mutual information J between $\mathbf{x}$ and $\mathbf{y}$ may be written as [8]

$$J = -\frac{1}{2}\log\det\{\mathbf{I} - \mathbf{K}\mathbf{K}^T\} = -\frac{1}{2}\sum_{i=1}^{m}\log(1 - k_i^2) \tag{8}$$

These equations indicate that the linear dependence and mutual information between the channels (blocks of two sonar returns) depend only on the the canonical correlations of the channels and may easily be computed after the decomposition. They also show that each canonical coordinate pair, e.g. (u_i, v_i), contributes to the linear dependence and mutual information according to its canonical correlation k_i. Thus, only canonical coordinates with large canonical correlations have significant contribution in the linear dependence and mutual information of the channels. Therefore, they are the only ones that need to be retained for classification tasks.

In most applications only the first few canonical coordinate pairs and their corresponding canonical correlations make a significant contribution in the linear dependence and mutual information of the channels. The conventional canonical coordinate decomposition in (3) requires computation of the square-root inverses of the covariance matrices $\mathbf{R}_{xx}$ and $\mathbf{R}_{yy}$ followed by the SVD of the coherence matrix $\mathbf{C}$. Moreover, the conventional method does not allow for extraction of a subset of canonical coordinates/correlations at a lower computational cost. These deficiencies make the conventional method inefficient for decomposition of large dimensional channels in real time applications.

It may easily be shown [11] that the canonical coordinate mapping matrices $\mathbf{W}$ and $\mathbf{D}$ are solutions to the generalized eigenvalue problems

$$\mathbf{R}_{xy}\mathbf{R}_{yy}^{-1}\mathbf{R}_{yx}\mathbf{W} = \mathbf{R}_{xx}\mathbf{W}\Sigma^2 \tag{9}$$

$$\mathbf{R}_{yx}\mathbf{R}_{xx}^{-1}\mathbf{R}_{xy}\mathbf{D} = \mathbf{R}_{yy}\mathbf{D}\Sigma^2 \tag{10}$$

or alternatively,

$$\mathbf{R}_{xy}\mathbf{D} = \mathbf{R}_{xx}\mathbf{W}\Sigma \tag{11}$$

$$\mathbf{R}_{yx}\mathbf{W} = \mathbf{R}_{yy}\mathbf{D}\Sigma \tag{12}$$

where $\Sigma^2 = \text{diag}(\sigma_1^2, \sigma_2^2, \ldots, \sigma_m^2)$ with $\sigma_1 \geq \sigma_2 \geq \cdots \geq \sigma_m > 0$ is the diagonal eigenvalue matrix.

In [11], an algorithm called the *alternating power method with deflation* has been reported that allows for recursive extraction of columns of $\mathbf{W}$ and $\mathbf{D}$. This algorithm is a two-step decomposition of the standard power iterations [12] for computing principal eigenvectors of a matrix and its convergence behavior follows that of the standard power iterations. Let $\mathbf{w}_i$ and $\mathbf{d}_i$ denote the *i*th columns of $\mathbf{W}$ and $\mathbf{D}$, respectively. These are the mapping vectors that map $\mathbf{x}$ and $\mathbf{y}$ to their *i*th canonical coordinates $u_i = \mathbf{w}_i^T\mathbf{x}$ and $v_i = \mathbf{d}_i^T\mathbf{y}$. The alternating power method starts by estimating $\mathbf{w}_1$ and $\mathbf{d}_1$. Given a random initial guess $\mathbf{d}_1(0)$, the first estimate of $\mathbf{w}_1$ is computed from (11). With this estimate of $\mathbf{w}_1$, (12) is used to compute a new estimate of $\mathbf{d}_1$. This iterative alternation between (11) and (12) continues until convergence. The corresponding canonical correlation k_1 may then be determined from $k_1 = \sigma_1 = \mathbf{w}_1^T\mathbf{R}_{xy}\mathbf{d}_1$. After estimating $\mathbf{w}_1$ and $\mathbf{d}_1$, the contribution of the generalized eigenvectors $\mathbf{w}_1$ and $\mathbf{d}_1$ is deflated [11] from the left hand sides of (11) and (12). As a result, a deflated version of the generalized eigenvalue problems in (11) and (12) is obtained with σ_2^2 as the largest eigenvalue and $\mathbf{w}_2$ and $\mathbf{d}_2$ as the principal generalized eigenvectors. Thus, the alternating power method may be used again to estimate $\mathbf{w}_2$, $\mathbf{d}_2$ and $k_2 = \sigma_2 = \mathbf{w}_2^T\mathbf{R}_{xy}\mathbf{d}_2$. This process may be continued until all dominant canonical correlations and canonical coordinate mapping vectors are extracted. This iterative algorithm does not require any matrix inversion or square-root computation.

III. Underwater Target Classification Using Canonical Correlations

In this section we first extract the canonical correlations associated with pairs of sonar returns in the wide-band ARL-UT data set. The extracted canonical correlations are subsequently used as features to classify mine-like objects from non-mine-like objects. The classification rates obtained using the canonical correlation features are then compared with those obtained using linear predictive coding (LPC) subband features [5],[7]. The scatter plots of the canonical correlation and the LPC subband features are presented to compare the discrimination power of each feature set.

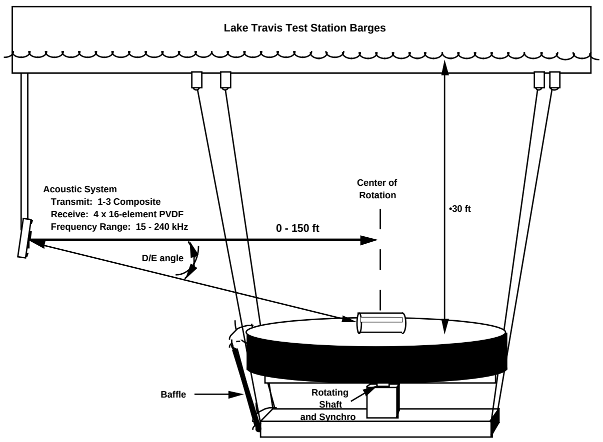

Fig. 1. Experimental Bottom Setup for the Wideband Data Set [13].

A. Wideband ARL-UT Data Set

The data set for our study is a subset of a broad-band acoustic data set collected at the ARL-UT Lake Travis test facility. This subset contains acoustic backscattered signals from three mine-like and three non-mine-like objects in two environmental conditions, namely, smooth and rough bottom. The rough bottom condition is similar to the smooth bottom, but the sand has been raked, giving it a rippled effect. The mine-like objects are two cylindrical steel objects, Target 6 and Target 7, and one truncated cone shape plastic object, Target 2. The non-mine-like objects are a drum, a concrete pipe and a telephone pole. During the data collection, the objects were placed on a rotating seabed, 25-30 feet below the water surface. The diameter of the seabed was 25 feet. The center of the object was positioned as near to the center of the circular platter as possible. While the object was being rotated with the plane of the seabed, the acoustic panel was set at depression/elevation (D/E) angle of 13.5 degrees. Backscattered signals were collected for 360 aspect angles with nearly uniform separation of 1 degree at a range of 105ft using a receiver array. A linear frequency modulated (LFM) transmit waveform with approximately 7 msec duration, sampled at 500 kHz, was used with a bandwidth of 85 kHz in the range of 15-100 kHz. The sonar returns were recorded for approximately 16 msec at 500 kHz, resulting in 8192 samples. Figure 1 shows the data collection setup. More details on the experimental conditions are given in [13]. In this study, we average the data of four channels of the receiver array to obtain a narrow beamwidth that mostly insonifies the region that includes the target/non-target object.

B. Feature Extraction Procedure

To build the ensembles of the two channels ($\mathbf{x}$ and $\mathbf{y}$) for canonical correlation analysis, we partition two backscattered signals, with certain aspect separation, of an object into overlapping blocks. The aspect separation between the two sonar returns must be chosen so that the reverberation effects are uncorrelated, while the returns from the object exhibit high coherence. The blocks of the first backscattered signal are taken as the samples of the first input channel (the $\mathbf{x}$-channel) and the blocks of the second backscattered signal are taken as the samples of the second input channel (the $\mathbf{y}$-channel). Thus, each realization of a channel is the vector of the time series associated with a block of range cells in the corresponding sonar return.

For the simulations performed here, the sonar returns paired into $(\mathbf{x}, \mathbf{y})$ channels according to aspect angles as follows: $\{1, 17\}$, $\{2, 18\} \cdots, \{344, 360\}, \{345, 1\}, \cdots,$ $\{360, 16\}$, corresponding to 16 degrees separation. The signals are partitioned into blocks of size 100 samples with 50 percent overlap. Using the alternating power method in [11] the first 15 (out of 100) canonical correlations associated with each pair are extracted. [1] These are the canonical correlations that have a large contribution to the linear dependence and mutual information between two sonar returns from an object. The extracted canonical correlations are then used as features to represent the backscattered signal associated with the first aspect angle in the corresponding pair. For example, the canonical correlations extracted from the aspect angles $\{2, 18\}$ is used as features for the sonar return at the aspect angle of 2 degrees.

The training set for the classifier is formed from the feature vectors extracted for 90 aspect angles of the *smooth bottom* data, at 4° steps. The feature vectors extracted from the rest of the aspect angles of the smooth bottom data (270 aspect angles) are kept to validate the trained classifier. We refer to this set as the validation set. This is the set that is usually used to evaluate the generalization capability of a trained classifier. To see how well the trained classifier performs when a completely new and unknown bottom condition is encountered, the trained classifier is tested on the features extracted from the backscattered signals of the *rough bottom* condition.

Figures 2(a)-(f) show the scatter plots of the first four features (the first four canonical correlations) for the training, validation and testing sets. As can be seen, for the training set (Figures 2(a),(d)) and validation set (Figures 2(b),(e)), the features of mine-like objects (Targets 2, 6 and 7) are packed together and almost completely separated from those of the non-mine-like objects (drum, concrete pipe, and telephone pole). Additionally, the extracted features for the training and validation sets for the objects on the smooth bottom, are fairly consistent.

In the rough bottom test condition (Figures 2(c),(f)), features of Target 2, Target 6, and the telephone pole stay in the same region as in the smooth bottom condition, while features of the drum and concrete pipe become more compact and move slightly towards the right side of the plot. Nonetheless, they still occupy almost the same regions as in training and validation sets. Features of Target 7, on the other hand, move from the upper right corner and spread out to the left side and mix with those of the drum and concrete

[1] All the initial estimates for columns of the matrices $\mathbf{W}$ and $\mathbf{D}$ are randomly selected. The number of iterations for the alternating power method is chosen to be 100.

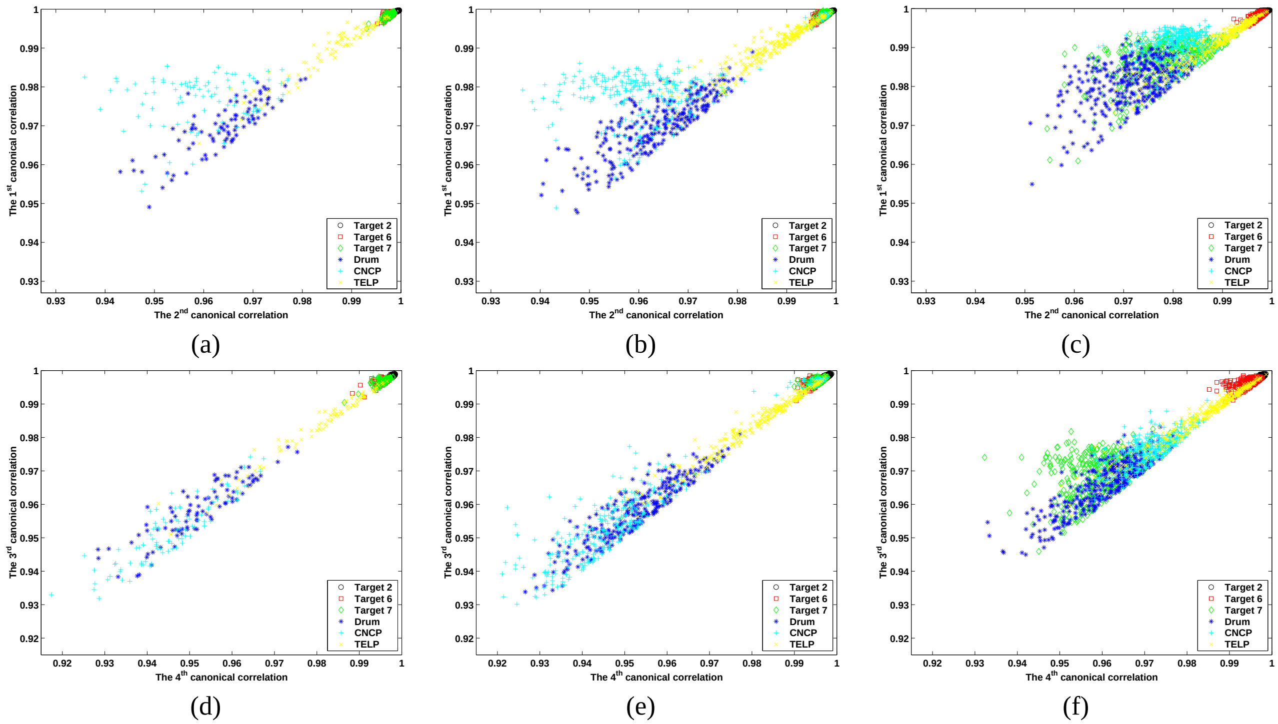

Fig. 2. Scatter plots of the ith vs. the jth canonical correlation for the training, validation and testing sets in the ARL-UT data set (a) Training set; $i = 1$ and $j = 2$. (b) Validation set; $i = 1$ and $j = 2$. (c) Testing set; $i = 1$ and $j = 2$. (d) Training set; $i = 3$ and $j = 4$. (e) Validation set; $i = 3$ and $j = 4$. (f) Testing set; $i = 3$ and $j = 4$.

pipe. Clearly, as will be shown in the next section, this leads to some degradation in the performance of the classifier in the rough bottom condition. These scatter plots clearly show that for 5 out of 6 objects canonical correlations are fairly robust to the changes in the bottom condition.

To further demonstrate the potential of canonical correlation features for separating targets and non-targets, we compare them with the LPC subband features of [5],[7]. To extract the LPC subband features for an object at a particular aspect angle, the matched filtered signal associated with that aspect angle is partitioned into several frequency subbands and a third order LPC model is fitted to each of the subband signals. The LPC coefficients extracted from all the subbands are then aggregated to represent the object at that particular aspect angle. Figures 3(a)-(f) show the scatter plots of four of the LPC subband features that offer the largest Fisher distance [14] between targets and non-targets. As can be seen, the LPC subband features for targets and non-targets are completely mixed together and it is very difficult to separate the two classes based on these features. At the same time, the canonical correlation features for targets and non-targets in Figures 2(a)-(f) are almost linearly separable, except for the rough bottom condition, where features of Target 7 undergo severe changes. These changes may be caused by secondary reflections and the large size of Target 7.

C. Classification Results

Subsequently, the extracted canonical correlation features may be used to train a back-propagation neural network (BPNN) to classify the mine-like objects (Targets 2, 6 and 7) from non-mine-like objects (drum, concrete pipe and telephone pole). To find a good network structure, eight different two-layer BPNN structures were tried. The number of hidden layer neurons was varied from 26 to 46. Each network was trained for ten different initializations. The training was performed for 10000 epochs, where an epoch was a complete run through the entire training set.

The best BPNN classifier (15-34-2), which was selected based on the average of the classfication percentages on training and validation sets, yields a correct classification rate of 99.1% on the training set, 98.6% on the validation set, and 81.5% on the testing set. These percentages are based on a hard-limiting decision threshold. Table I benchmarks our classification results against those in [5],[7], obtained using the LPC subband features. The confusion matrices obtained for these classifiers are shown in Table II (for the canonical correlation features) and Table III (for the LPC subband features). The results clearly demonstrate the potential of

TABLE I

CLASSIFICATION RESULTS OBTAINED USING CANONICAL CORRELATION FROM LPC SUBBAND FEATURES.

Features	Training	Validation	Testing
Canonical correlation	99.1%	98.6%	81.5%
LPC subband	99.6%	82.5%	75.2%

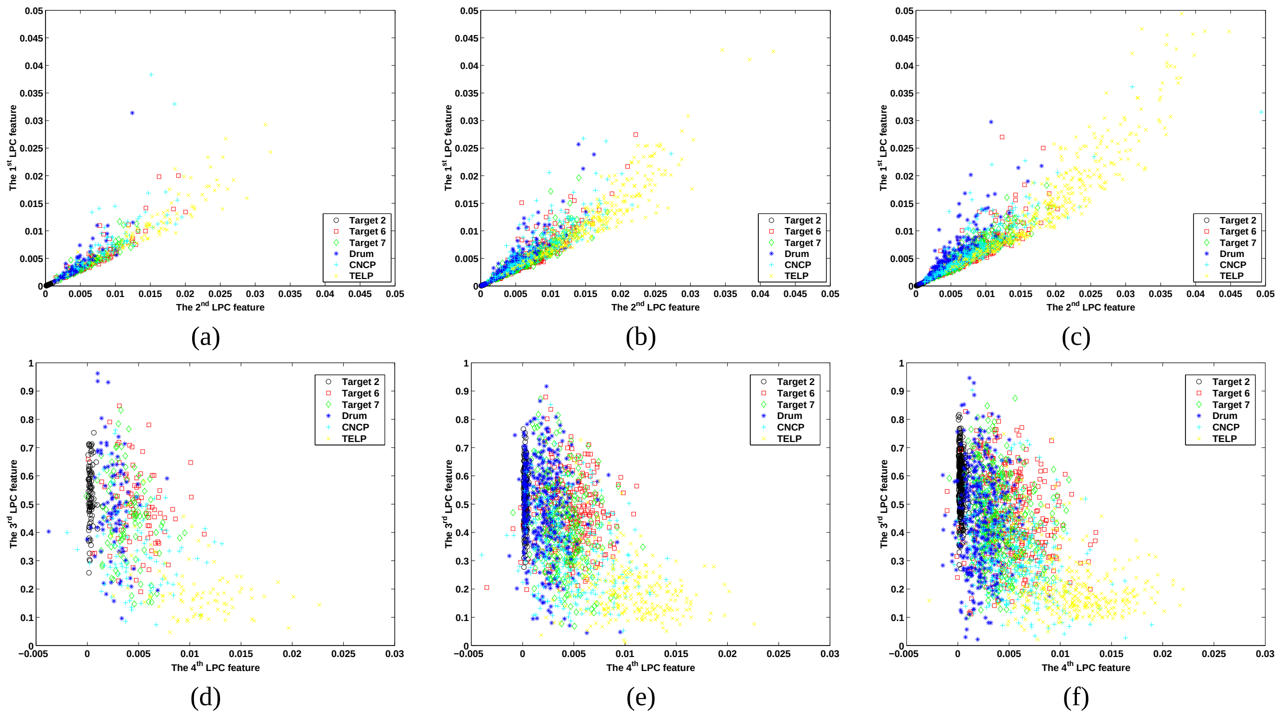

Fig. 3. Scatter plots of the ith vs. the jth LPC subband features for the training, validation and testing sets in the ARL-UT data set. The LPC subband features are arranged in descending order of their Fisher distance. (a) Training set; $i = 1$ and $j = 2$. (b) Validation set; $i = 1$ and $j = 2$. (c) Testing set; $i = 1$ and $j = 2$. (d) Training set; $i = 3$ and $j = 4$. (e) Validation set; $i = 3$ and $j = 4$. (f) Testing set; $i = 3$ and $j = 4$.

the canonical correlation features for classifying targets from non-targets in difficult bottom conditions.

TABLE II

CONFUSION MATRIX FOR THE CLASSIFIER TRAINED WITH THE CANONICAL CORRELATION FEATURES

	Validation Set		Testing Set	
Object	Target	Non-Target	Target	Non-Target
Target 6	270	0	355	5
Target 7	268	2	1	359
Target 2	270	0	358	2
Drum	0	270	0	360
Concrete Pipe	0	270	0	360
Telephone Pole	21	249	33	327

TABLE III

CONFUSION MATRIX FOR THE CLASSIFIER TRAINED WITH THE LPC SUBBAND FEATURES

	Validation Set		Testing Set	
Object	Target	Non-Target	Target	Non-Target
Target 6	215	55	224	136
Target 7	177	93	214	146
Target 2	265	5	349	11
Drum	57	213	128	232
Concrete Pipe	56	214	92	268
Telephone Pole	17	253	22	338

It is interesting to note that the classifier trained using canonical correlation features correctly classifies Target 2 and Target 6 at almost all aspect angles in both smooth and rough bottom conditions, while the classifier trained using the LPC subband features has poor performance on these targets. Additionally the canonical correlation features provide substantially lower false alarm rates (2.6% for validation and 3.1% for testing) compared to the LPC subband features (16.1% for validation and 22.4% for testing). However, the classifier trained with the LPC subband features has better performance for target 7 in the rough bottom condition compared to the canonical correlation-based classifier. This is due to the fact that in the rough bottom condition, the canonical correlation features of Target 7 undergo severe changes and mix with those of the drum and concrete pipe (Figures 2(c),(f)).

IV. CONCLUSIONS AND FUTURE WORK

Canonical coordinate decompositions have been used to extract the coherent features that exhibit coherence across sonar returns. These features are the dominant canonical correlations associated with the returns. The hypothesis behind this feature extraction method is that for certain aspect separations linear dependence or coherence between the sonar returns reveals common target/non-target attributes, whereas linear independence reveals bottom reverberation features. This hypothesis has been validated on the ARL-UT data set. For this data set, the extracted canonical correlations offer very good separation between mine-like and non-mine-like objects. They are also robust (except for Target 7) to changes in the bottom conditions.

The feature extraction method proposed here is based on the analysis of linear dependence between the sonar returns. In some cases the linear dependence alone may not be sufficient to acquire enough information for detection/classification. One possible solution is to implicitly map the sonar returns into higher dimensional subspaces induced by nonlinear kernels [15]. The canonical correlation analysis in the kernel domain may then reveal higher order features that may be coherent between the sonar returns. This approach is currently under investigation [16].

ACKNOWLEDGEMENTS

The data and technical support were provided by the NSWC, Coastal Systems Station, Panama City, FL., and the Applied Research Laboratory, University of Texas, Austin, TX.

REFERENCES

[1] M. R. Azimi-Sadjadi, D. Yao, Q. Huang, and G. J. Dobeck, "Underwater target classification using wavelet packets and neural network," *IEEE Trans. Neural Networks*, vol. 11, pp. 784–794, May 2000.

[2] D. Li, M. R. Azimi-Sadjadi, and G. J. Dobeck, "Comparison of different classification paradigms for underwater target disccrimination," *To Appear In IEEE Trans. Neural Networks*.

[3] M. R. Azimi-Sadjadi, D. Yao, A. Jamshidi, and G. J. Dobeck, "Underwater target classification in changing environments using an adaptive feature mapping," *IEEE Trans. Neural Networks*, vol. 13, pp. 1099–1111, Sept. 2002.

[4] M. R. Azimi-Sadjadi, D. Yao, D. Li, A. Jamshidi, and G. J. Dobeck, "Comparison of effects of sonar bandwidth for underwater target classification," *IEEE J. Oceanic Engineering*, vol. 27, pp. 619–627, July 2002.

[5] M. R. Azimi-Sadjadi, M. Robinson, A. Jamshidi, and G. J. Dobeck, "A biologically inspired adaptive underwater target classification using a multi-aspect decision feedback unit," *Oceans 2002 MTS/IEEE*, vol. 1, pp. 38–45, Oct. 2002.

[6] A. Pezeshki, M. R. Azimi-Sadjadi, L. L. Scharf, and M. Robinson, "A canonical correlation-based feature extraction method for underwater target classification," *Oceans 2002 MTS/IEEE*, vol. 1, pp. 29–36, Oct. 2002.

[7] M. Robinson, "Different multi-aspect fusion systems for underwater target classification," Master Thesis, Colorado State University, Fort Collins, CO 80523-1373, USA, Feb. 2002.

[8] L. L. Scharf and C. T. Mullis, "Canonical coordinates and the geometry of inference, rate, and capacity," *IEEE Trans. on Signal Processing*, vol. 48, pp. 824–831, March 2000.

[9] L. L. Scharf and J. T. Thomas, "Wiener filters in canonical coordinates for transform coding, filtering, and quantizing," *IEEE Trans. on Signal Processing*, vol. 46, pp. 647–654, March 1998.

[10] M. L. Eaton, *Multivariate Statistics: A Vector Space Approach*. New York: Wiley, 1983, ch. 10.

[11] A. Pezeshki, L. L. Scharf, M. R. Azimi-Sadjadi, and Y. Hua, "Two-channel constrained least squares problems: Solutions using power methods and connections with canonical coordinates," *Submitted to IEEE Trans. Signal Processing*, April 2003.

[12] G. H. Golub and C. F. V. Loan, *Matrix Computations*, 3rd ed. Baltimore, MD: John Hopkins Univ. Press, 1996.

[13] ARL-UT, "Target data acquisition setup," Applied Research Lab, University of Texas, Austin, USA, Manual.

[14] R. O. Duda and P. E. Hart, *Pattern Classification and Scene Analysis*. New York: Wiley, 1973.

[15] B. Schölkopf and A. J. Smola, *Learning with Kernels, Support Vector Machines, Regularization, Optimization, and Beyond*. Cambridge, MA: MIT Press, 2002.

[16] A. Pezeshki, M. R. Azimi-Sadjadi, and L. L. Scharf, "Kernel-based canonical coordinate decomposition of two-channel nonlinear maps," *In Preparation*.